# Synthesis and Characterization of Silica-Supported Boron Oxide Catalysts for the Oxidative Dehydrogenation of Propane

Alyssa M. Love<sup>†</sup>, Melissa C. Cendejas<sup>†</sup>, Brijith Thomas<sup>§</sup>, William P. McDermott<sup>†</sup>, Pajean

Uchupalanun<sup>†</sup>, Catherine Kruszynski<sup>†</sup>, Samuel P. Burt<sup>‡</sup>, Theodore Agbi<sup>‡</sup>, Aaron J. Rossini<sup>\*, §</sup>,

and Ive Hermans<sup>\*,†‡</sup>

- † Department of Chemistry, University of Wisconsin Madison, 1101 University Avenue,

  Madison, Wisconsin 53706, United States
- Department of Chemical and Biological Engineering, University of Wisconsin Madison,
   1415 Engineering Drive, Madison, Wisconsin 53706, United States

§ US DOE Ames Laboratory, Ames, Iowa, 50011, United States

Department of Chemistry, Iowa State University, 2438 Pammel Drive, Ames, Iowa, 50011,
United States

**Abstract.** In this contribution we report on the oxidative dehydrogenation (ODH) activity of silica-supported boron oxide prepared via incipient wetness impregnation. Characterization of pristine and spent catalysts with infrared, Raman, and solid-state NMR spectroscopy reveals the presence of both isolated and aggregated oxidized boron sites. The results of these investigations, in combination with our earlier work on bulk boron-containing ODH catalysts (*e.g.*, h-BN, metal borides, and elemental boron), give direct evidence that oxidized boron species formed *in situ* on the surface of these materials are responsible for the exceptional catalytic behavior. We anticipate that investigation of supported boron materials can provide insight into the structural characteristics required for selective boron-containing ODH catalysts.

#### 1. Introduction

In recent years, hexagonal boron nitride (h-BN) and other boron-containing (bulk) materials have been reported as highly selective catalysts for the oxidative dehydrogenation (ODH) of light alkanes to olefins.<sup>14</sup> For all of these active materials, X-ray photoelectron spectroscopy (XPS) and InfraRed spectroscopy revealed the formation of oxidized boron species on the surface of the materials following catalytic testing for the ODH of propane.<sup>14</sup> We recently investigated spent h-BN ODH catalysts using (multidimensional) solid-state NMR spectroscopy, X-ray absorption spectroscopy (XAS), and scanning electron microscopy (SEM).<sup>8</sup> This work revealed the formation of an amorphous oxidized/hydrolyzed boron layer consisting of threefold coordinate boron sites with a general formula  $B_2(OH)_{2x}O_{3-x}$  (x = 0-3) to account for varying numbers of hydroxyl and bridging oxide groups coordinated to each boron atom within this phase. Although we observe an induction period during which the oxide layer forms, these observations do not allow us to irrefutably conclude that the  $B_2(OH)_{2x}O_{3-x}$  layer contains the

active sites, or if the formation of this  $B_2(OH)_{2x}O_{3-x}$  layer is a consequence of the reaction. The synthesis of a catalyst with a more structurally controlled oxidized boron phase could serve to enhance our understanding of boron-containing materials during ODH and could therefore potentially lead to the synthesis of improved catalysts.

To understand the role of the oxide phase, here we have synthesized a series of silicasupported boron oxide materials via incipient wetness impregnation of a triisopropyl borate
(B(OPr),) solution in isopropanol and subsequent calcination in air. These materials are shown to
selectively convert propane to propylene under ODH conditions. The fact that these B/SiO,
materials are active for the ODH of propane gives direct evidence that the oxidized boron layer is
indeed active for ODH, which we hypothesized based on our aforementioned characterization
studies on h-BN and other boron-containing ODH catalysts. In addition, this is in line with
observations from previous work that reports supported boron oxide materials (e.g., boron oxide
supported on alumina) as catalysts for the ODH of light alkanes.

Although those materials
were reported to leach boron under the reaction conditions – likely because of the high nominal
loading of up to 30 wt. % B<sub>2</sub>O/Al<sub>2</sub>O<sub>3</sub> – we reimagine such supported boron oxide materials as a
potential route to the next generation of B-containing ODH catalysts with tunable surface
speciation.

We characterize the B/SiO<sub>2</sub> materials with a combination of infrared (IR), Raman, and solid-state NMR spectroscopy to develop a detailed understanding of the boron surface sites present on these catalysts. Based on our experience with supported metal oxides, 15-17 we synthesized materials with a series of boron loadings that would potentially generate species ranging from well-dispersed, isolated boron sites at low loadings, to boron oxide-type agglomerates at higher loadings. In this way, trends in the materials' catalytic behavior could be correlated with the

types of surface species (from isolated to aggregated sites) present on the materials, similar to the case for silica-supported vanadium oxide." In reality, the dispersion of boron on the support, and hence the resultant surface sites on these materials, is far more complex than originally anticipated. We also characterized the spent B/SiO<sub>2</sub> catalysts following catalytic testing for ODH of propane with the same characterization methods and found that restructuring of the boron sites on the silica surface takes place. As is also the case for the h-BN catalysts, the surface boron phase on these B/SiO<sub>2</sub> catalysts during ODH appears to restructure. These experimental observations are in line with a recent computational study that predicted the formation of a highly dynamic oxide phase on the surface of h-BN under reaction conditions." While these studies have enhanced our understanding of these materials' catalytic behavior, the complexity of the oxide phase formed on this material presents a significant challenge for determining the exact catalyst features required for high ODH selectivity.

## 2. Experimental

## 2.1 Materials Synthesis.

The materials X B/SiO<sub>2</sub> (where X corresponds to the B loading) were synthesized via incipient wetness impregnation. Prior to impregnation, silica (Aerosil<sup>3</sup> 300 from Evonik, specific surface area of 300 m<sup>2</sup> g<sup>3</sup>) was dried under static conditions overnight at 120 °C. Impregnation was performed inside a glovebox under a dry N<sub>2</sub> atmosphere. A solution of triisopropyl borate (B(OPr)<sub>3</sub>; Sigma-Aldrich) in dry isopropanol (Sigma-Aldrich; 99.5 %) was prepared with such a ratio of B(OPr)<sub>3</sub> to isopropanol so as to achieve a boron loadings from ca. 0.25 to 2 wt. %, while using a total solution volume equal the pore volume of the support (1.4 mL solution per 1g of Aerosil<sup>3</sup> 300). This solution was then added dropwise to the silica support. The impregnated

sample was transferred to a calcination oven where it calcined to 550 °C at 1 °C min<sup>-1</sup> under dry air and held at 550 °C for 3 h.

#### 2.2 Catalytic Testing.

The B/SiO<sub>2</sub> catalysts were compressed using a pellet press (Pike Technologies; pressure program: 1 ton of force for 10 s and 2 tons of force for 10 s.) and sieved to collect particles of 300-600 µm diameter in order to limit any potential mass transfer effects.<sup>19</sup> About 25-50 mg B/SiO<sub>2</sub> was diluted in quartz chips in a 1:2 ratio and loaded into a quartz reactor tube (8 mm ID) and supported on a bed of quartz wool in the middle of the tube. Additional quartz wool was used to pack the inside of the quartz tube lightly past the catalyst bed to reduce dead volume and minimize the potential for homogeneous gas-phase reactions. Flow rates of C<sub>1</sub>H<sub>8</sub> (instrument grade, Matheson), O<sub>2</sub> (UHP, Airgas) and N<sub>2</sub> (UHP, Airgas) were controlled using three mass flow controllers (Bronkhorst) and calibrated to each individual gas to allow total flow rates of 40 -200 mL min<sup>-1</sup>. The H<sub>2</sub>O produced from the reaction was condensed using a thermoelectricallycooled condenser held at -5 °C. The dried reactor effluent was monitored using an on-line  $\mu$ GC (Inficon Micro GC Fusion Gas Analyzer) equipped with three GC modules and three micro thermal conductivity detectors ( $\mu$ TCD). O<sub>2</sub>, N<sub>2</sub>, CH<sub>4</sub>, and CO were analyzed using a Rt-Molsieve 5A column, CO<sub>2</sub> was analyzed using an Rt-U-Bond column, and all hydrocarbons apart from CH<sub>4</sub> were analyzed using an Rt-Alumina Bond/Na<sub>2</sub>SO<sub>4</sub> column.

In each catalytic test, the reactor was heated to the reaction temperature of 500 °C under O<sub>2</sub> and N<sub>2</sub> flow. The temperature was controlled using a thermocouple inserted into the middle of the catalyst bed. After the temperature was stabilized, the C<sub>3</sub>H<sub>8</sub> feed was introduced and GC measurements were begun. As there is an induction period in which excess boron leaches from the catalyst surface before catalytic activity is stabilized, each catalyst was treated for 24 hours

under a feed of 6:3:11 C<sub>3</sub>H<sub>8</sub>:O<sub>2</sub>:N<sub>2</sub> at 40 mL min<sup>-1</sup>. After this treatment, the gas flow rate was adjusted to give WHSV<sup>-1</sup> values ranging from 0.6 – 6.3 kg<sub>-sat</sub> s mol<sub>C3H8</sub><sup>-1</sup> (ca. 40-200 mL min<sup>-1</sup>) and further GC measurements were performed. Reported experiments showed the carbon balance closed within ±3%.

#### 2.3 Materials Characterization.

*ICP-MS*. Inductively coupled plasma-mass spectrometry measurements were performed by the Trace Elements Laboratory at the Wisconsin State Hygiene Lab, using an ICP-MS instrument outfitted with HF-resistant components. Prior to analysis, 10-15 mg of X B/SiO<sub>2</sub> sample was digested in 100  $\mu$ L of 48 wt. % HF and diluted in 20 mL of Milli Q H<sub>2</sub>O. Samples were diluted again by a factor of 50 prior to ICP-MS analysis.

IR Spectroscopy. Prior to analysis, all samples were dehydrated at 500 °C in a flow of air overnight. IR spectra were recorded on a self-supporting wafer using a Bruker Alpha spectrometer in transmission mode (resolution of 2 cm<sup>-1</sup>). Intensities were normalized to the Si-O-Si overtones of the silica framework. Analysis was carried out inside a glovebox (<1 ppm of H<sub>2</sub>O and O<sub>2</sub>).

Raman Spectroscopy. In situ Raman measurements were carried out with a Renishaw InVia Raman spectrometer with a 785 nm excitation laser. All measurements used a 1200 l mm<sup>4</sup> grating and were taken with a range of 250-1200 cm<sup>4</sup> and a dispersion of 1.36565 cm<sup>4</sup> pixel<sup>4</sup>. Each sample was loaded in a high-temperature Linkam CCR1000 cell and heated at 10 °C/min under air to 500 °C, stopping every 100 °C to record Raman spectra. The spectra are reported without any background subtraction.

*NMR (UW-Madison)*. Solid state NMR experiments were performed on a Bruker standard-bore 11.7 T ( $v_0(\cdot H) = 500$  MHz) NMR spectrometer equipped with Bruker Avance III console and with a Bruker 4 mm broad band HX MAS probe. The samples were packed into a 4 mm rotor in an inert nitrogen atmosphere glove box and MAS experiments were performed with nitrogen gas. 1D "B solid state NMR spectra were obtained with a 1D double echo (DEPTH) sequence for suppression of background signals using a composite pulse ( $\pi/2 - \tau - \pi - \tau - \pi - \tau - \text{acquire}$ ) with a recycle delay of 4s.

NMR (Iowa State). Solid state NMR experiments were performed on a Bruker Wide-bore 9.4 T  $(v_0(H) = 400 \text{ MHz})$  NMR spectrometer equipped with Bruker Avance III HD console and with a Bruker 2.5 mm broad band HXY MAS probe. The samples were packed in to a 2.5 mm rotor after grinding to powders in an inert nitrogen atmosphere glove box. MAS experiments were performed with nitrogen gas to prevent hydration. The spectra were collected with a MAS frequency of 25000 Hz at room temperature. 1D "B solid-state NMR spectra were obtained with a rotor synchronized spin echo pulse sequence  $(\pi/2 - \tau - \pi - \tau$ -acquire). The echo delays  $(\tau)$ were fixed to three-rotor cycles to help suppress the probe background. CT-selective "B rf pulse widths were calibrated with a spin echo experiment on boron nitride nanotubes obtained from Sigma Aldrich. CT selective  $\pi/2$  pulse of 8  $\mu$ s which correspond to "B rf field of 18 kHz were used (Figure S14). "B chemical shifts were indirectly referenced to the established chemical shift standards using the previously reported relative NMR frequencies.<sup>20</sup> The SPINAL-64 scheme with an rf field of 100 kHz was used for H heteronuclear decoupling in the spin echo experiments.21 1H rf pulses were directly calibrated on the samples, and the chemical shifts were referenced to neat tetramethylsilane by the use of admantane ( $\delta_{10}(H) = 1.82$  ppm) as a secondary

chemical shift standard. All experiments on the same nucleus have been processed with the same window function parameters for a quantitative comparison of the signal to noise ratio (SNR). B NMR spectra of catalysts were processed with 150 Hz exponential line broadening. Simulations of all MAS B solid-state NMR spectra were performed in the solid line shape analysis (SOLA) module v2.2.4 included in the Bruker Topspin v4.0.1 software.

The proton detected dipolar refocused insensitive nuclei enhanced by population transfer (D-RINEPT) spectra were acquired with the pulse sequence described in the previous literature.<sup>22</sup> <sup>24</sup> In D-RINEPT experiments, the symmetry based recoupling sequence super-cycled (S)R4<sub>1</sub><sup>2</sup> was applied to the 'H nuclei. The rf field for the SR4<sub>1</sub> recoupling was set to two times the sample spinning rate to fulfill the second order rotor resonance recoupling condition. The second order R<sup>3</sup> condition was precisely calibrated by varying the rf field of the spin lock pulse in a simple <sup>1</sup>H 90° pulse-spin lock pulse sequence. The length of the recoupling sequence was optimized directly on the samples of interest and the time providing the most intense signal was chosen. The total recoupling duration  $(4m \times \tau_t)$  was 1.28 ms. RAPT was used to enhance the sensitivity of <sup>11</sup>B → <sup>1</sup>H D-RINEPT NMR experiments.<sup>25,26</sup> RAPT was implemented with WURST pulses that were 80 µs in duration separated by 2 µs applied at frequency offsets of ±400 kHz.27 The frequency sweep range of the WURST was 25 kHz and the "B rf field was approximately 50 kHz."B{'H dephased} spectra were collected with a separate local field (SLF) type pulse sequence with 8 k scans and a recycle delay of 1 s.28 SR412 dipolar recoupling was applied during the first echo delay with a H rf field of 50 kHz. The dipolar recoupling sequence was applied for 0.8 or 1.2 ms to dephase "B signals that are coupled to protons.

#### 3. Results/Discussion

# 3.1 Synthesis and catalytic testing of B/SiO<sub>2</sub> for ODHP

The synthesis of silica-supported boron oxide was carried out analogous to the incipient wetness impregnation of vanadium on silica." A solution of triisopropyl borate (B(OPr),) in isopropanol was added dropwise to an amorphous silica support (Aerosil\* 300; BET surface area ca. 300 m² g²). Following the impregnation step, the material was calcined in air at 550 °C (ramp rate of 1 °C · min²) for 3 h. The concentration of B(OPr), in solution was adjusted to achieve boron loadings between 0.25 and 2 wt. %. Samples are named X B/SiO, (where X = wt. % B) according to their initial boron loading as determined by inductively coupled plasma-mass spectrometry (ICP-MS). We emphasize that 2 wt. % is the maximum boron loading that can be achieved with this preparation method. Indeed, due to the volatility of the boron precursor, any additional boron precursor that cannot readily react with the silica support will evaporate from the surface during calcination before it has a chance to anchor. Following calcination of these materials, each was tested as a catalyst for the oxidative dehydrogenation of propane (ODHP) at 500 °C.

Figure 1a shows the propylene selectivity as a function of propane conversion for ODHP over the series of five different B/SiO<sub>2</sub> catalysts. ODH experiments were performed in a fixed bed reactor under a flow of C<sub>2</sub>H<sub>8</sub>, O<sub>2</sub>, and N<sub>2</sub> (in a molar ratio of 6:3:11) at 500 °C (see experimental section for details). The materials were exposed to ODH conditions for 24 h prior to varying catalyst contact times to collect the propylene selectivity versus conversion trend, then discontinuing the experiment to perform materials characterization. The selectivity versus conversion for h-BN is also shown for comparison. The conversion-selectivity trends for each of the B/SiO<sub>2</sub> materials appears to fall on a similar line. This line has a very similar slope to the h-

BN conversion-selectivity trend; however, the overall selectivity to propylene is ca. 10% less for the B/SiO<sub>2</sub> materials. For example, Figure 1b compares the product distributions for h-BN and 0.58 B/SiO<sub>2</sub> at iso-conversion (ca. 5% propane conversion). The overall selectivity to propylene for h-BN at this conversion is 88%, whereas the overall selectivity for 0.58 B/SiO<sub>2</sub> is 77%. 0.58 B/SiO<sub>2</sub> forms more ethylene (14%, compared to 7.7% for h-BN), CO (5.5% compared to 2.6% for h-BN), and CO<sub>2</sub> (1.6% compared to 0.25% for h-BN). We attribute the lower propylene selectivity of the B/SiO<sub>2</sub> materials to the silica support, as the presence of pure silica seems to have a deleterious effect on propylene selectivity for h-BN catalysts as well (Figure S1). Nevertheless, the catalytic behavior of the B/SiO<sub>2</sub> materials at such low B loadings is remarkable considering that under reaction conditions bare SiO<sub>2</sub> is inert.

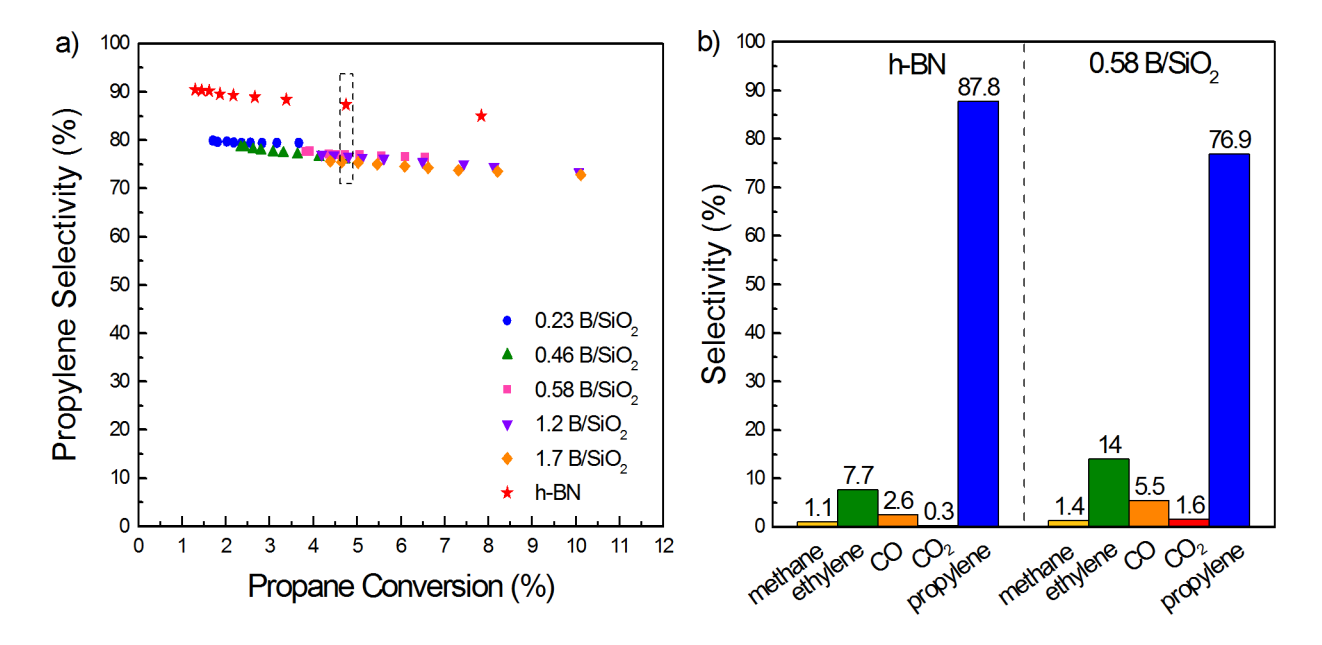


**Figure 1.** a) Propylene selectivity versus propane conversion data for the oxidative dehydrogenation (ODH) of propane over a series of B/SiO<sub>2</sub> catalysts (0.23, 0.46, 0.58, 1.2, and 1.7 wt. % B) and h-BN. Different conversions were achieved by changing the gas flow rate

between 40 and 200 mL min<sup>-1</sup>. b) Product distribution comparison at iso-conversion (5 % propane conversion) for h-BN and 0.58 B/SiO<sub>2</sub>.

Previous literature for supported boron oxide materials indicates that boron oxide can leach from the surface of solid oxide supports like alumina upon treatment at high temperatures.<sup>10-14</sup> Therefore, in order to assess these catalysts' stabilities, the boron content for each sample was determined with ICP-MS after calcination of the materials (denoted 'fresh') as well as after 24 h of catalytic testing for ODHP (denoted 'spent', Figure 2). While 0.23 B/SiO<sub>2</sub> does not appear to have any significant reduction in boron content after catalytic testing, materials with a higher initial boron loading lose a larger fraction of their original boron content. In fact, following 24 h on stream, 1.7 B/SiO<sub>2</sub> has decreased in boron loading by approximately two-thirds to 0.65 wt. % boron. While the boron content in these materials decreases somewhat drastically after the first 24 h on stream, it does not appear that this decrease continues until all boron is stripped from the catalyst surface. An analysis of the propane conversion as a function of catalyst time-on-stream shows that all of the materials reach a constant propane conversion after about 24 h, and that level of conversion correlates with the boron content after 24 h (Figure S2). We hypothesize that during this induction period, the surface boron species restructure to a more stable phase (vide infra) while some weakly bound boron leaches off the surface. This, of course, warrants a detailed structural analysis of these catalysts which will be outlined in the following section.

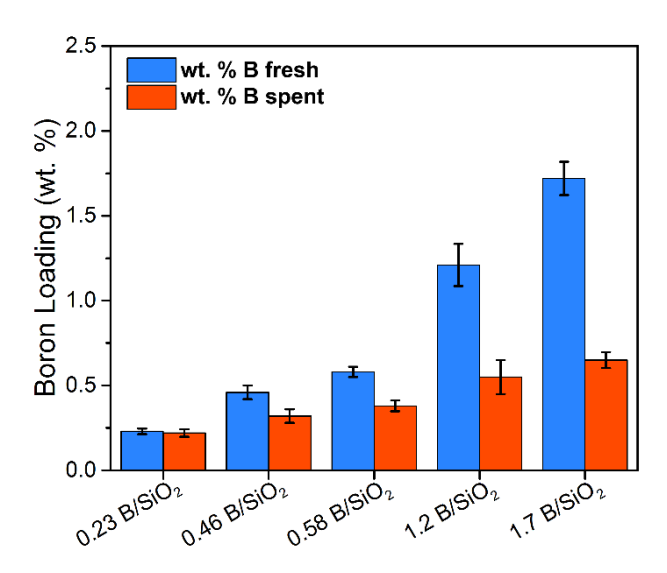


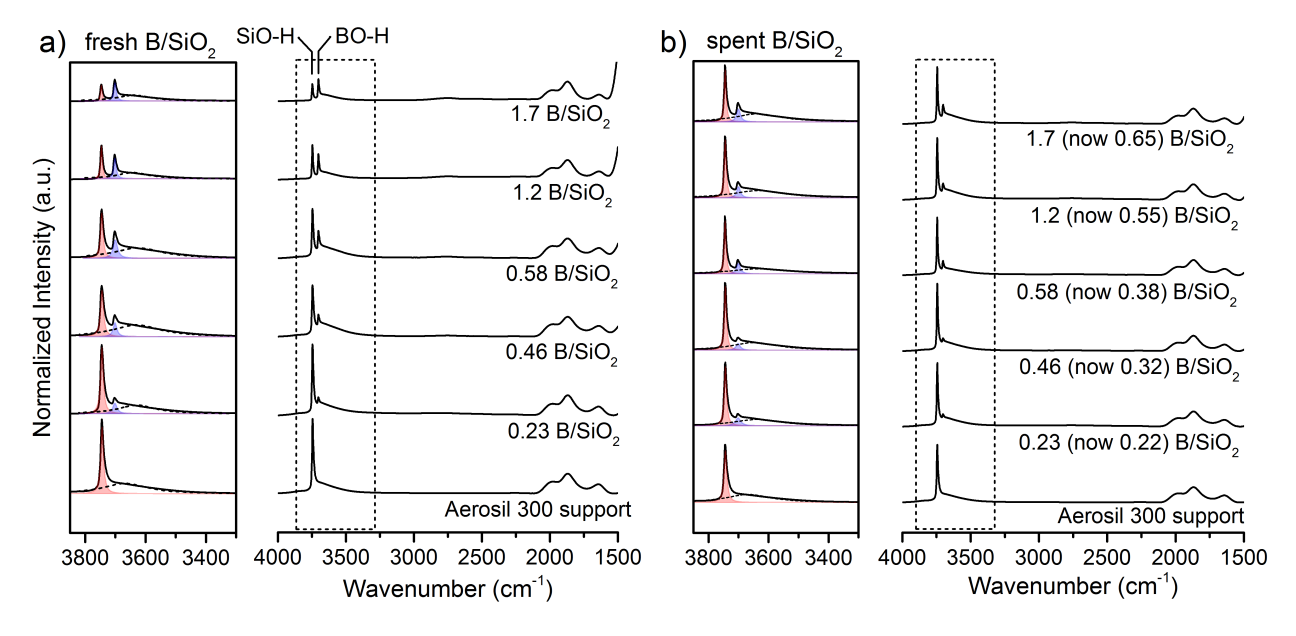
**Figure 2.** Summary of ICP-MS elemental analysis results for fresh (left bars, blue) and spent (right bars, orange) B/SiO<sub>2</sub> catalysts.

#### 3.2 Structural characterization of boron sites on B/SiO<sub>2</sub> materials.

Fresh and spent B/SiO<sub>2</sub> catalysts were characterized with a combination of IR, Raman, and solid-state NMR spectroscopy. A summary of identified B surface sites and the techniques used to identify them are provided in Table 1 at the end of this discussion.

Figure 3a shows the transmission IR spectra for the series of fresh B/SiO<sub>2</sub> catalysts. All materials were dehydrated at 500 °C in air prior to analysis in order to assess the structure of the materials after exposure to ODH reaction temperatures. The intensities of each spectrum were normalized to the Si-O-Si overtones observed between 1500 and 2100 cm<sup>3</sup>. The spectrum of the dehydrated Aerosil<sup>3</sup> 300 support is also provided for reference. Each of the B/SiO<sub>2</sub> materials in Figure 3a contains a stretch at 3745 cm<sup>3</sup> and 3701 cm<sup>3</sup> that correspond to isolated Si-OH and B-OH vibrations, respectively.<sup>29,31</sup> Each spectrum also contains a shoulder at ca. 3650 cm<sup>3</sup> that corresponds to hydrogen-bonded hydroxyl groups on the material, although the exact nature of the hydrogen bonding (SiOH - SiOH, SiOH - BOH, BOH - BOH, or some combination) is unclear from these spectra alone.

The deconvolutions of the fresh B/SiO<sub>2</sub> IR spectra (using one broad Lorentz peak to approximate the shoulder around 3650 cm<sup>4</sup>) are shown in the panel on the left side of Figure 3a, and a summary of the peak areas as a function of boron content are provided in Figure S3. Since these transmission IR spectra are normalized to the same features, we can use these deconvolutions to assess the differences in relative quantities of each vibrational species on these materials. As expected, the number of isolated SiOH groups decreases with increasing boron loading. We also see an increase in isolated BOH groups on the materials until 0.58 B/SiO<sub>2</sub>; after higher loadings, the area of this feature appears to decrease slightly, and levels off above 0.58 wt. % B.



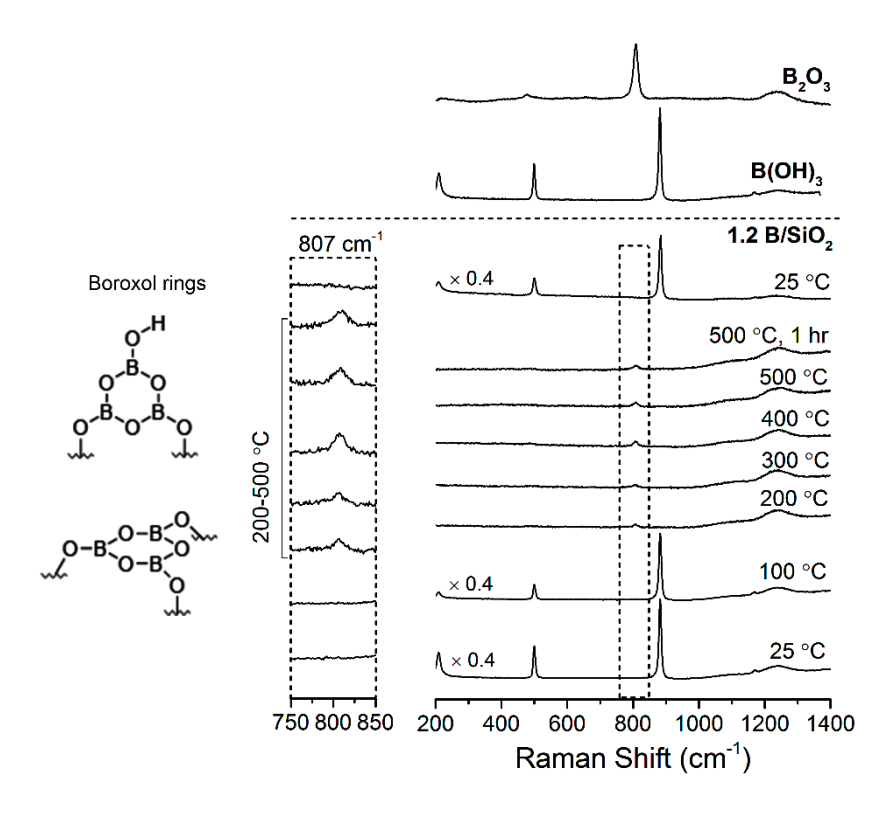
**Figure 3.** a) Normalized transmission FTIR spectra for (from bottom to top) Aerosil® 300 silica, fresh 0.23, 0.46, 0.58, 1.2 and 1.7 B/SiO<sub>2</sub> samples dehydrated at 500 °C in air, and b) transmission IR of the same samples after propane ODH testing for 24 h (Aerosil® 300 spectrum included again for comparison).

Figure 3b shows the IR spectra for the same materials following catalytic testing for propane ODH for 24 h on stream. The spent materials are named by the same loading as their fresh counterparts (*e.g.*, 'fresh 0.46 B/SiO<sub>2</sub>' becomes 'spent 0.46 B/SiO<sub>2</sub>'), although the actual boron content of the spent materials significantly decreases, as shown in Figure 2. Following catalytic testing, the spent B/SiO<sub>2</sub> samples were dehydrated at 500 °C in air prior to IR analysis. Like the fresh materials, all of the spectra contain peaks at 3745 cm<sup>3</sup> and 3701 cm<sup>3</sup> and a small shoulder at ca. 3650 cm<sup>4</sup>. However, the relative quantities of these features are far different from their fresh counterparts. In particular, spent 0.58 B/SiO<sub>2</sub>, spent 1.2 B/SiO<sub>2</sub>, and spent 1.7 B/SiO<sub>2</sub> have far more isolated silanols and fewer B-OH groups than their analogous fresh materials. We attribute this to the significant loss of boron on these materials (as shown in Figure 2) and subsequent regeneration of Si-OH following boron leaching from the surface. The lower loading samples, such as spent 0.23 B/SiO<sub>2</sub> and spent 0.46 B/SiO<sub>2</sub>, still have similar relative Si-OH and B-OH peak intensities to their fresh counterparts, which we attribute to the lesser extent of boron leaching.

We utilized Raman spectroscopy to obtain complimentary vibrational information on the boron sites on silica. Figure 4 shows the Raman spectra for the *in situ* dehydration of fresh 1.2 B/SiO<sub>2</sub> to 500 °C in air. At ambient conditions, the Raman spectrum for fresh 1.2 B/SiO<sub>2</sub> contains peaks at 209, 500, and 882 cm<sup>4</sup> that match closely with vibrations observed in the Raman spectrum for boric acid (shown above the spectra for 1.2 B/SiO<sub>2</sub> in Figure 4). The vibration at 209 cm<sup>4</sup> has been previously attributed to a lattice-translatory oscillation in boric acid, whereas the peaks at 500 cm<sup>4</sup> and 882 cm<sup>4</sup> correspond to O-B-O bending and B-O stretching modes, respectively.<sup>22,33</sup> Upon dehydration of 1.2 B/SiO<sub>2</sub> at temperatures > 100 °C, these features disappear and instead a small feature at 807 cm<sup>4</sup> can be observed. This is very close to the feature at 808 cm<sup>4</sup> observed in B<sub>2</sub>O<sub>3</sub> (top spectrum in Figure 4). A full-intensity spectrum of the 1.2 B/SiO<sub>3</sub> dehydrated at 400 °C

is shown in Figure S4. Based on literature Raman studies of borate and borosilicate glasses, this feature is specifically attributed to the symmetric breathing mode for six-membered boroxol rings. This feature persists in the Raman spectrum for fresh 1.2 B/SiO<sub>2</sub> upon heating to 500 °C and holding for 1 h. Additionally, this feature persists after a second cycle of hydration-dehydration (Figure S5). Interestingly, the same features are observed in the Raman spectra after dehydration of the other fresh B/SiO<sub>2</sub> samples with loadings less than 1 wt. % B (Figure S6).

A similar *in situ* Raman dehydration study was also attempted for spent 1.2 wt. % B/SiO<sub>2</sub> (and spent 0.58 wt. % B/SiO<sub>2</sub>; Figure S7). However, the representative ambient temperature Raman spectrum for spent 1.2 B/SiO<sub>2</sub> shows only a small feature at 882 cm<sup>-1</sup>, and upon dehydration only features from the silica support can be observed. This decrease in Raman sensitivity could be due to a decreased boron loading for spent 1.2 B/SiO<sub>2</sub> to 0.55 wt. % B following catalytic testing for 24 h on stream, however, we achieved sufficient Raman sensitivity on fresh 0.46 B/SiO<sub>2</sub> and fresh 0.58 B/SiO<sub>2</sub> to observe the boroxol ring feature at 807 cm<sup>-1</sup> (Figure S6). Therefore, we hypothesize that the lack of an observable feature at 807 cm<sup>-1</sup> in the spent materials may be due to the degradation of these boroxol ring species during catalytic testing, either through the loss of boron content or by restructuring to metaborate species.



**Figure 4.** *In situ* Raman study on the dehydration of fresh 1.2 B/SiO<sub>2</sub> to 500 °C in air. The top spectrum for 1.2 B/SiO<sub>2</sub> labeled 25 °C was taken after re-exposure of the sample to ambient conditions following dehydration. Spectra of boric acid (B(OH)<sub>3</sub>) and boron oxide (B<sub>2</sub>O<sub>3</sub>) are provided for comparison.

All of the fresh and spent B/SiO<sub>2</sub> samples were also analyzed with solid-state "B magic angle spinning (MAS) NMR. Figure 5 shows a summary of all the 1D MAS "B solid-state NMR spectra for the fresh (panel a) and spent (panel c) B/SiO<sub>2</sub>. The "B solid-state NMR spectra were obtained with a double echo (DEPTH) pulse sequence to suppress NMR signals from the probe background." All samples were dehydrated at 500 °C in air prior to analysis and NMR rotors were packed in a glovebox to prevent re-hydration before the NMR experiments. All of the "B NMR spectra for fresh B/SiO<sub>2</sub> have similar features spanning from ca. 20 ppm to 0 ppm and can be simulated with central transition "B MAS powder patterns that are characteristic of trigonal

planar BO<sub>3</sub> sites. The observed feature at 194.2 eV in XPS for each of these materials is also consistent with BO<sub>3</sub> sites (Figure S8).<sup>7</sup> Based on the typical peak shape for a single three-coordinate boron site,<sup>37</sup> it appears that the fresh materials contain multiple types of BO<sub>3</sub> units (*i.e.*, coordination of both oxide and hydroxide anions to the boron).

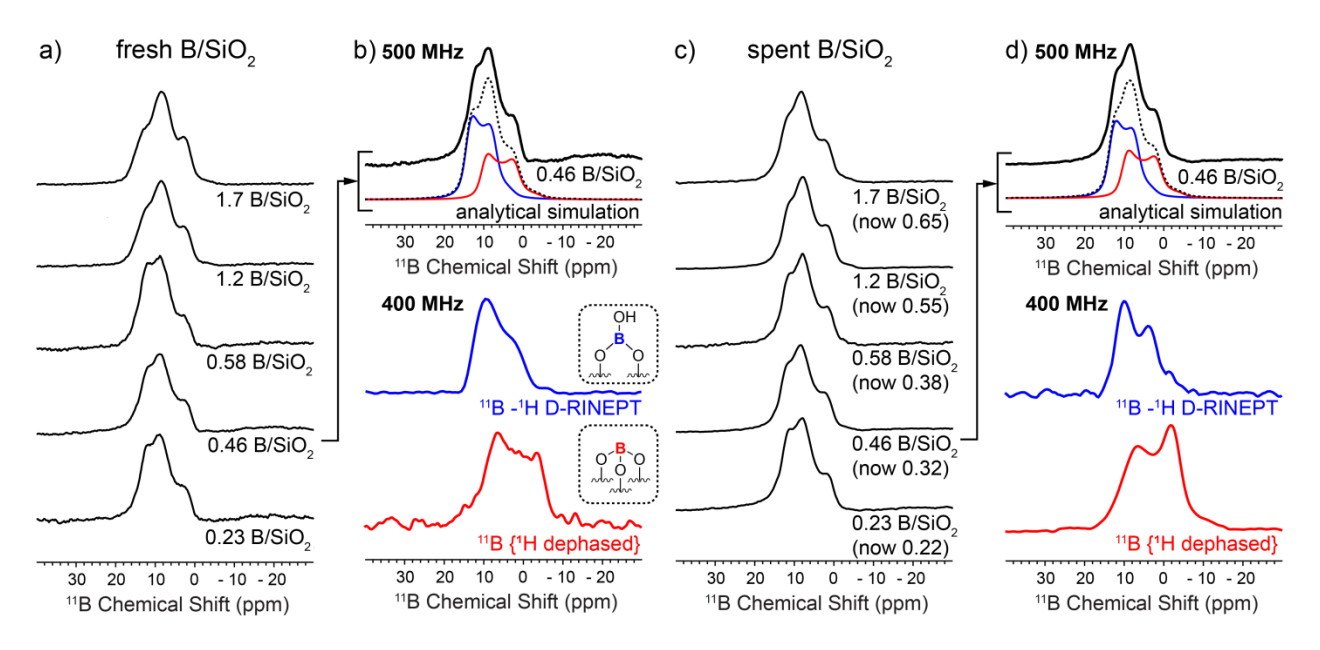


Figure 5. a) 1D MAS <sup>11</sup>B solid-state NMR spectra for fresh 0.23, 0.46, 0.58, 1.2, and 1.7 B/SiO<sub>2</sub> materials, b) sample deconvolution for fresh 0.46 B/SiO<sub>2</sub> (top trace), <sup>11</sup>B→<sup>1</sup>H D-RINEPT spectrum for fresh 0.46 B/SiO<sub>2</sub> (middle trace) with structural assignment (inset), and <sup>11</sup>B{<sup>1</sup>H dephased} spectrum for fresh 0.46 B/SiO<sub>2</sub> (bottom trace) with structural assignment (inset) and c) 1D MAS <sup>11</sup>B solid-state NMR spectra for the same materials following catalytic testing (spent; new loadings are 0.22, 0.32, 0.38, 0.55, 0.65 wt.% B, respectively). d) Analogous deconvolutions, <sup>11</sup>B→<sup>1</sup>H D-RINEPT, and <sup>11</sup>B {<sup>1</sup>H dephased} NMR spectra for spent 0.46 B/SiO<sub>2</sub> (loading 0.32 wt. % B after catalytic testing). Spectra taken at 500 MHz (11.7 T) and 400 MHz (9.4 T) were collected with magic angle spinning (MAS) rates of 10 kHz and 25 kHz, respectively.

Analytical simulations of these spectra were used to determine the isotropic shift ( $\delta_{\text{iso}}$ ; analogous to chemical shifts measured in solution NMR) and the electric field gradient (EFG) tensor parameters – the quadrupolar coupling constant ( $C_{\text{o}}$ ) and the EFG tensor asymmetry parameter ( $\eta_{\text{o}}$ ). The EFG tensor parameters provide information about the coordination environment of the "B nuclei in the sample. We note here that the isotropic shift values can be approximated by reading the ppm value at the onset of the left side of the powder pattern (not at the center), however, analytical simulations of the spectra are needed to accurately determine the value for  $\delta_{\text{iso}}$ .

Simulation of the fresh 0.46 B/SiO, "B NMR spectrum (Figure 5b, top trace) fits well with two powder patterns with  $\delta_{100}$  values at 15.9 and 12.3 ppm. We note that because of the nature of the amorphous support and based on the variety of species identified (vide infra), there likely exists a small distribution of isotropic shifts. However, for ease of analysis and discussion, we simulate the <sup>1</sup>B 1D spectra using only two peaks. The C₀ values for these two patterns are 2.4 and 2.6 MHz, respectively, and  $\eta_0$  for both peaks is 0. The rest of the fresh B/SiO<sub>2</sub> materials can also be fit with two patterns where  $\delta_{iso} = 15.8-15.9$  ppm and  $C_{iso} = 2.3-2.4$  MHz for the first, and  $\delta_{iso} =$ 12.3-12.4 ppm and  $C_0 = 2.6-2.7$  MHz for the second; the main difference between the spectra of fresh B/SiO<sub>2</sub> materials with variable B loading is that the relative integrated intensity of each pattern varies from a ratio of approximately 1:1 to 2.1:1 for the high and low shift patterns, respectively (Figure S9, Table S1). The magnitude of C<sub>o</sub> for both patterns indicates that all boron reside in BO<sub>3</sub> units with trigonal planar geometry. 38.39 We expect that the differences in  $\delta_{100}$  for the two features in the 1D "B spectra arise from differences in number of hydroxyl groups on the boron nuclei in these materials. The presence of a hydroxyl group has a known effect on the  $\delta_{10}$ for oxidized boron species. Boric acid (B(OH)<sub>3</sub>), for example, has a reported δ<sub>150</sub> of 18.8 ppm,<sup>40</sup>

whereas boron oxide ( $B_2O_3$ ) has a reported  $\delta_{180}$  of 14.6.<sup>38</sup> Further experiments to verify these hypotheses are explained below.

We performed 'B-'H double resonance NMR experiments on select B/SiO<sub>2</sub> materials (0.46) B/SiO<sub>2</sub> and 1.2 B/SiO<sub>2</sub>) in order to obtain further information on the structure of the oxidized boron species. The double resonance 'H-"B NMR experiments were performed with a 400 MHz (9.4 T) NMR spectrometer, whereas the 1D MAS "B NMR spectra in Figure 5a (and 5c) were obtained with a 500 MHz (11.7 T) NMR spectrometer, which leads to slight differences in the breadths of the "B powder patterns. Regardless of the field used for acquisition, similar values for  $\delta_{10}$ ,  $C_{0}$ , and  $\eta_{0}$  were determined, validating the analytical simulations. The middle (blue) trace in Figure 5b shows a proton-detected "B NMR spectrum obtained with the dipolar refocused insensitive nuclei enhanced by polarization transfer (D-RINEPT) pulse sequence<sup>22,23</sup> for fresh 0.46 B/SiO<sub>2</sub>. This experiment selectively shows "B nuclei proximate to protons which should correspond to "B nuclei with hydroxyl groups attached (see inset next to D-RINEPT spectrum). Interestingly, the D-RINEPT spectrum can be fit to a peak with  $\delta_{100} = 15.8$  ppm,  $C_0 = 2.4$  MHz, and  $\eta_{\mbox{\tiny 0}}=0.0,$  which matches the high frequency pattern obtained from simulations of the 1D spin echo spectrum acquired at 11.7 T. Based on the 500 °C dehydration temperature for this material, most of these hydroxylated boron species are expected to have only one hydroxyl group. The bottom trace in Figure 5b shows the "B {'H dephased} spin echo spectrum for fresh 0.46 B/SiO<sub>2</sub>. This experiment gives complementary information to the D-RINEPT experiment in that it shows the "B spectrum for "B nuclei distant from protons (i.e., containing no hydroxyl groups; see inset next to "B{'H dephased} spectrum). This spectrum can also be fit with  $\delta_{so}$  and EFG tensor parameters close to those for the low frequency (red) pattern in the simulations of the "B 1D spin echo NMR spectrum of fresh 0.46 B/SiO<sub>2</sub>.

Based on the experiments outlined above, we can conclude that the fresh 0.46 B/SiO<sub>2</sub> materials consist of a mixture of trigonal planar BO<sub>3</sub> units with and without hydroxyl groups attached. We also performed the same experiments on the fresh 1.2 B/SiO<sub>2</sub> material and observed a similar match between the features in the analytical simulation of the spin echo, D-RINEPT and "B {¹H dephased} spectra (Figure S10 and Figure S11). Therefore, we expect that the features deconvoluted from the remaining fresh B/SiO<sub>2</sub> 1D "B spectra all correspond to BO<sub>3</sub> structures with and without hydroxyl groups.

A similar "B NMR analysis was carried out to evaluate the spent B/SiO<sub>1</sub> materials. Figure 5c shows the "B spin echo NMR spectra for the spent B/SiO<sub>1</sub> samples following catalytic testing for propane ODH. Much like the fresh materials, the "B spin echo NMR spectra of the spent materials can be simulated with two major features, with one example shown for spent 0.46 B/SiO<sub>1</sub> in Figure 5d. Analytical simulations for the remaining spent materials are provided in Figure S9, and simulation parameters are summarized in Table S1. All the spent B/SiO<sub>2</sub> materials can be simulated with one pattern with  $\delta_m = 14.8$ -15.0 ppm,  $C_o = 2.3$ -2.4 MHz, and  $\eta_o = 0.0$ , and a second pattern with  $\delta_m = 12.1$ -12.4 ppm,  $C_o = 2.6$ -2.7 MHz, and  $\eta_o = 0.0$ . D-RINEPT and "B {'H dephased} spin echo NMR spectra of the spent 0.46 B/SiO<sub>2</sub> material verify that the features in the spin echo simulation correspond to a combination of BO<sub>3</sub> units with and without hydroxyl groups attached (Figure 5d). These structural assignments were also verified for spent 1.2 B/SiO<sub>2</sub> (Figure S10). The slight changes in  $\delta_m$ , in particular for the hydroxylated BO<sub>3</sub> species, may be indicative of restructuring of the material upon catalytic testing. This will be discussed in further detail in the following section.

#### 3.3 Multidimensional solid-state NMR.

Aside from the observation of boroxol rings in the Raman spectra for fresh B/SiO<sub>2</sub>, thus far we only have information on the immediate bonding environment of the boron surface sites on our materials. The surface consists of trigonal planar BO<sub>3</sub> units with a mixture of sites with and without hydroxyl groups. Since it is difficult to resolve subtle differences in the connectivity of the boron species on the catalyst surface with 1D NMR experiments alone (*i.e.*, are the BO<sub>3</sub> sites mostly isolated or are they connected through bridging B-O-B moieties), we utilize a series of 2D NMR experiments on select low loading (0.46 B/SiO<sub>2</sub>) and high loading (1.2 B/SiO<sub>2</sub>) catalysts to obtain further information on the interaction between different sites on the catalyst surface.

Figure 6 displays the 2D 'H-'H double quantum-single quantum (DQ-SQ) NMR experiments double for fresh 0.46 B/SiO, and 1.2 B/SiO, This experiment selectively detects only those 'H signals proximate (dipole coupled) to other 'H nuclei. For both spectra, the SQ frequency is provided on the horizontal axis, whereas the DQ frequency is provided on the vertical axis. Signals appear in the indirect dimension at a DQ frequency equal to the sum of the SQ frequency of the two correlated 'H spins. The diagonal dotted line in both spectra represents the position on the 2D NMR contour plot in which the DQ frequency is exactly double the SQ frequency. Signals appearing on this line correspond to autocorrelations which arise when pairs of 'H spins with the same chemical shift are proximate to one another.

Figure 6a shows the 2D 'H-'H DQ-SQ spectrum for fresh 0.46 B/SiO<sub>2</sub>. A 'H spin echo spectrum that displays all the 'H signals in the sample is also provided for comparison above the projection of the 'H-'H SQ frequency. The 'H spin echo spectrum for fresh 0.46 B/SiO<sub>2</sub> shows an intense peak at 1.6 ppm and a less intense peak at 2.7 ppm that correspond to protons from isolated Si-OH and B-OH groups, respectively. Proton detected 2D 'H{20Si} cross polarization heteronuclear

correlation (CP HETCOR)<sup>43</sup> and <sup>11</sup>B→<sup>1</sup>H D-RINEPT experiments verify that the 1.6 ppm and 2.7 ppm proton signals are proximate to "Si and "B nuclei, respectively (Figures S12 and S13). The <sup>1</sup>H SQ projection of the 2D <sup>1</sup>H DQ-SQ spectrum of 0.46 B/SiO<sub>2</sub> shows one peak at 1 ppm and a broader peak centered at ca. 4 ppm. This spectrum represents the 1D proton spectrum filtered to display only signals from 'H spins proximate to other 'H spins. Both the 'H 1 ppm and 4 ppm SQ peaks exhibit DQ auto-correlations at twice the SQ chemical shift, suggesting they are proximate to other protons of the same type. Based on the chemical shift for each of these proton signals in the SQ frequency dimension, we attribute the cross peak between 1 ppm H signals to intermolecular (through-space) DQ coherence between hydrogen bonded Si-OH groups on the surface. However, based on the IR spectrum and the 'H spin echo spectrum for this material, we know that the majority of SiOH groups on this material are isolated. By the same logic, we attribute the auto-correlation cross peak between 4 ppm 'H signals to B-OH groups hydrogen bonded or adjacent to one another on the surface. Since some B-OH groups are sufficiently close to one another to give rise to DQ NMR signals, we expect that a subset of the hydroxylated boron species on fresh 0.46 B/SiO<sub>2</sub> is connected by bridging oxide (B-O-B) bonds. The assignments for these cross peaks are illustrated in Figure 6a.

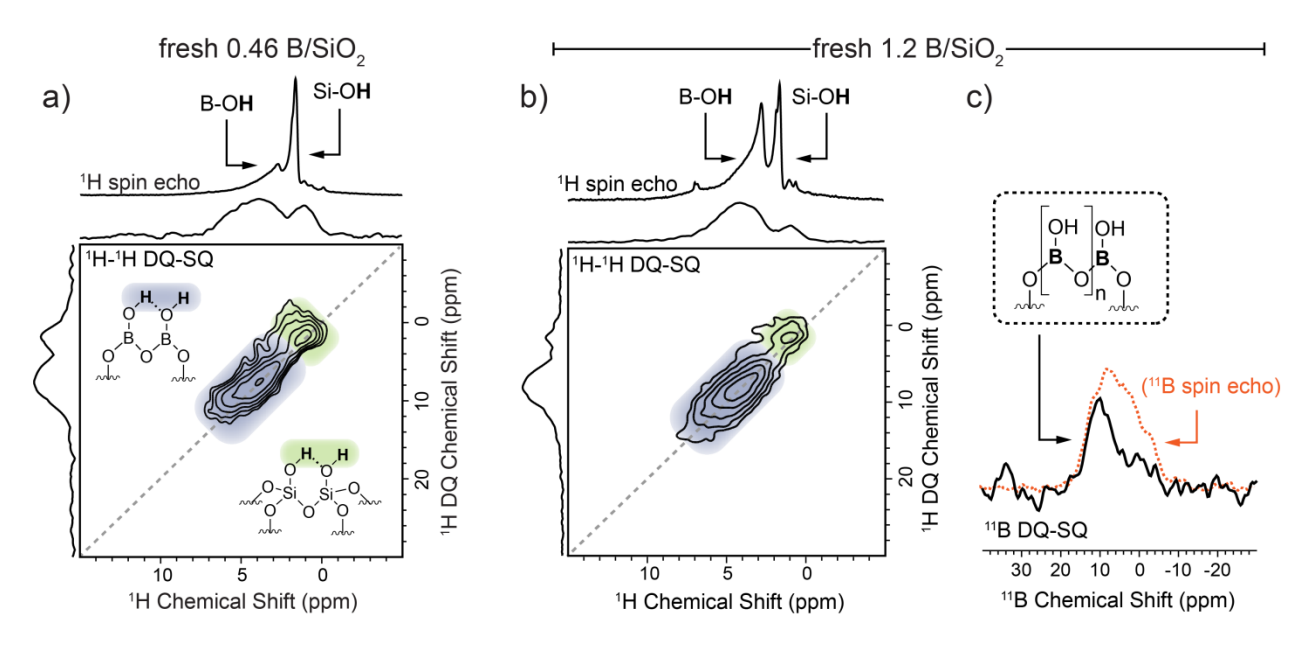


**Figure 6.** 2D <sup>1</sup>H-<sup>1</sup>H double quantum-single quantum (DQ-SQ) NMR spectra for a) fresh 0.46 B/SiO<sub>2</sub> and b) fresh 1.2 B/SiO<sub>2</sub>. <sup>1</sup>H spin echo NMR spectra are provided on the horizontal axis of the 2D spectra for comparison. Assignments for the cross peaks in panels a) and b) are color-coded to the structures in panel b). c) 1D DQ-SQ filtered <sup>11</sup>B NMR spectrum with structural assignment (inset).

Figure 6b shows the 'H-'H DQ-SQ NMR spectrum for fresh 1.2 B/SiO<sub>2</sub>. Again, the 'H spin echo for fresh 1.2 B/SiO<sub>2</sub> is provided above the horizontal axis in order to compare the standard 1D 'H NMR spectrum with the DQ-SQ filtered spectrum below it. The 'H spin echo spectrum for fresh 1.2 B/SiO<sub>2</sub> also contains two major peaks at 1.6 ppm and 2.7 ppm (with a slight shoulder at higher frequencies, see below) that correspond to protons on Si-OH and B-OH groups, respectively. In 1.2 B/SiO<sub>2</sub> the B-OH 'H NMR signal is of similar intensity as the Si-OH signal. This matches with observations of the quantities of Si-OH and B-OH vibrational species in transmission IR (Figure 3). The increased quantity of B-OH (compared to 0.46 B/SiO<sub>2</sub>) is expected given the higher boron content on the silica surface. When we examine the 2D 'H-'H

DQ-SQ NMR spectrum for 1.2 B/SiO<sub>2</sub>, we observe the same auto-correlation cross peaks between <sup>1</sup>H signals at 1 ppm and 4 ppm that we attribute to H-bonded Si-OH groups and H-bonded B-OH groups, respectively. We emphasize that the most intense sharp features at 1.6 and 2.7 ppm in the <sup>1</sup>H spin echoes for 0.46 and 1.2 B/SiO<sub>2</sub> do not appear in the DQ filtered spectrum. This indicates that there is a combination of isolated *and* hydrogen bonded SiOH and BOH groups present on the surface of these materials. This observation is corroborated by the combination of sharp bands at 3745 cm and 3701 cm<sup>-1</sup> and the small broad shoulder at 3650 cm<sup>-1</sup> observed in the IR spectra for these materials (see Figure 3).

Figure 6c shows the 1D "B DQ-filtered NMR spectrum" for fresh 1.2 B/SiO₁. This experiment shows only "B nuclei proximate to other "B nuclei. The "B-DQ filtered spectrum shows an "B NMR signal that matches the high frequency pattern of the "B spin echo (see dotted orange spin echo spectrum overlaid on black DQ-SQ spectrum). The "B→'H D-RINEPT spectrum of fresh 1.2 B/SiO₁ indicates the high frequency pattern from the "B spin echo spectrum must correspond to "B nuclei with hydroxyl groups attached. Therefore, on the basis of the homonuclear 'H and "B DQ NMR experiments, we conclude that some of the surface boron sites exist as H-bonded B-OH species connected by a bridging oxide group. We note here that the "B DQ NMR experiment is highly non-quantitative and has only 1-2 % efficiency as compared to an "B spin echo NMR experiment. Therefore, although we expect the majority of boron species that are interconnected by bridging oxide bonds contain hydroxyl groups, it is still possible that, to a lesser extent, there are some boron species without hydroxyl groups that could be interconnected − *e.g.*, boroxol ring species like those observed with Raman spectroscopy (Figure 4). Based on the NMR studies in Figure 6, it appears that the surface of the fresh B/SiO₁ catalysts predominantly contain chains of

interconnected "B sites with hydroxyl groups (similar to chain-type metaborate structures observed in borate glasses") at both high and low loadings, in addition to isolated boron sites.

As was described above, elemental analysis shows that after ODH catalytic testing the B/SiO<sub>2</sub> catalysts lose some boron content, with the loss being more drastic in the samples of higher loading. We analyzed spent 0.46 B/SiO<sub>2</sub> and 1.2 B/SiO<sub>2</sub> samples with <sup>1</sup>H and <sup>11</sup>B NMR experiments to assess any structural changes on the B/SiO<sub>2</sub> materials following catalytic testing. Both spent materials exhibit similar attributes, therefore we will limit our discussion here to spent 0.46 B/SiO<sub>2</sub>. The analogous experiments on spent 1.2 B/SiO<sub>2</sub> are shown in Figure S14. Like the fresh B/SiO<sub>2</sub> materials, the spent materials contain a mixture of three-coordinate BO<sub>3</sub> units with and without hydroxyl groups attached (Figure 5).

Figure 7a displays the 2D "B → H D-RINEPT NMR spectrum for spent 0.46 B/SiO<sub>2</sub>. The 1D "H spin echo spectrum is also shown on the horizontal axis. The "H spin echo spectrum of spent 0.46 B/SiO<sub>2</sub> shows peaks at 1.6 ppm and 2.7 ppm that are from isolated Si-OH groups and B-OH groups attached to three coordinate BO<sub>3</sub> units, respectively. The IR spectrum for spent 0.46 B/SiO<sub>2</sub> also indicates there are small quantities of isolated B-OH (Figure 3). Notably, the "H spin echo spectrum for spent 0.46 B/SiO<sub>3</sub> shows two additional peaks at 7 and 8.4 ppm that were absent from the spectrum of fresh 0.46 B/SiO<sub>3</sub>. The 2D "B → H INEPT spectrum also shows a lower intensity "H peak at 8.4 ppm which correlates to a relatively sharp "B NMR signal centered at ca. 0 ppm. Given the peak position and shape for this "B feature, we attribute this signal to a four-coordinate boron signal. Therefore, we assign the "H signal at 8.4 ppm to a hydroxyl group on a four-coordinate BO<sub>4</sub> nucleus. Interestingly, no appreciable signal from BO<sub>4</sub> sites are observed in the 1D "B spectrum of spent B/SiO<sub>4</sub> materials (Figure 5). We note that the "B → H INEPT experiment is non-quantitative, as different sites will have different dipolar couplings and

"B  $T_1$  and  $T_2$  relaxation times. The "B NMR signals of the four-coordinate sites are likely absent from the 1D "B spectra because these sites may have a long "B  $T_1$  because of their small  $C_{\infty}$ . Hence, the four-coordinate boron species are detected in the D-RINEPT experiment but not in the 1D "B experiment. However, we do believe the observation of these species is evidence for the restructuring of the surface boron species as a result of exposure to ODH catalytic conditions.

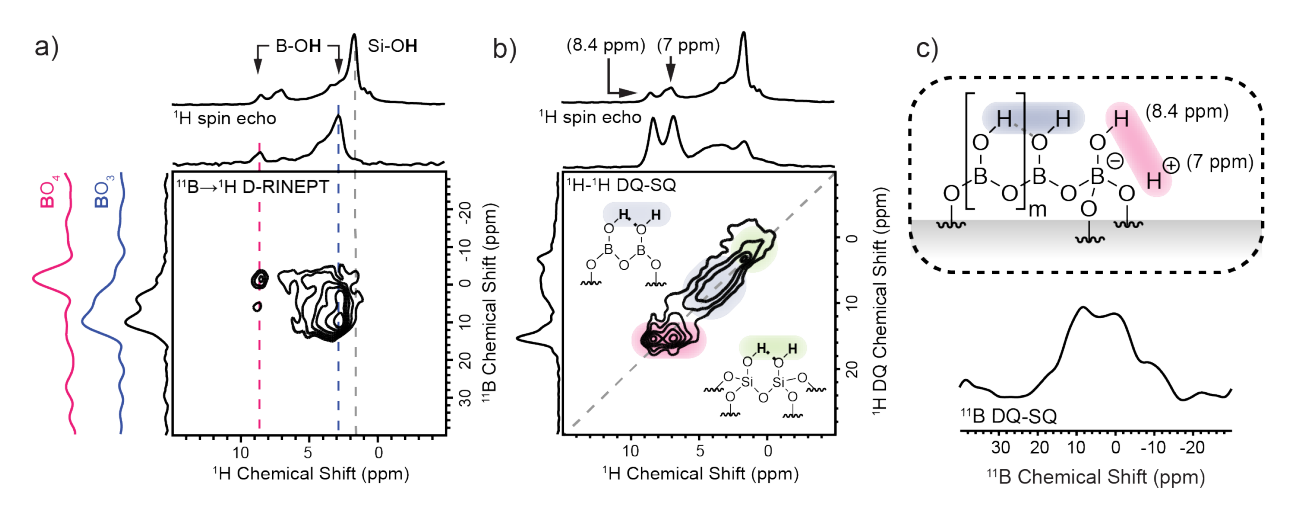


**Figure 7.** a) 2D <sup>11</sup>B→<sup>1</sup>H D-RINEPT NMR spectra for spent 0.46 B/SiO<sub>2</sub>. Projections at different points along the spectrum are shown stacked above the total projection on the vertical axis. b) <sup>1</sup>H<sup>1</sup>H Double Quantum-Single Quantum (DQ-SQ) NMR spectrum for spent 0.46 B/SiO<sub>2</sub> c) 1D DQSQ filtered <sup>11</sup>B NMR spectrum for spent 0.46 B/SiO<sub>2</sub>. A proposed structural assignment for the proton signals is shown in the inset. <sup>1</sup>H spin echo spectrum is provided on the horizontal axis of the 2D spectra in panels a) and b).

A 2D 'H-'H DQ-SQ NMR experiment was also performed on spent 0.46 B/SiO<sub>2</sub>. Figure 7b shows the 'H-'H DQ-SQ NMR spectrum for spent 0.46 B/SiO<sub>2</sub>. The 2D contour plot for spent 0.46 B/SiO<sub>2</sub> still contains cross peaks on the diagonal (where the frequency in the DQ dimension is exactly twice the SQ dimension frequency) associated with 'H signals at 1 and 4 ppm, which we again assign to H-bonded Si-OH and B-OH groups, respectively. A strong DQ coherence is

observed between the peaks at 7 ppm and 8.4 ppm (DQ dimension shift of 15.4 ppm), implying that these two hydrogen atoms are spatially proximate. The "B→'H D-RINEPT experiments suggest that at least one of these proton signals (at 8.4 ppm) is associated with a BO<sub>i</sub>-type species. 'H-"Si CP HETCOR experiments show that the signal at 7 ppm is not nearby the "Si nuclei (Figure S15), nor would we expect such a high chemical shift proton signal to be associated with a Si-OH type species." We suggest a potential structural assignment for these anomalous proton signals in the inset in Figure 7 based on structures proposed for on aluminasupported boron materials. However we suspect that the formation of these species is indicative of surface restructuring and are likely not a significant contributor to the catalytic properties of these materials. For comparison, the oxidized boron phase in hexagonal boron nitride following ODH catalytic testing does not appear to contain significant amounts of four-coordinate boron.'

Figure 7c contains the 1D "B DQ filtered NMR spectrum for spent 0.46 B/SiO<sub>2</sub>. This experiment was run with the same conditions (and same number of scans) as the "B DQ-SQ NMR spectrum for fresh 1.2 B/SiO<sub>2</sub> in Figure 6c. The fact that this material contains ca. 25 % of the boron content of fresh 1.2 B/SiO<sub>2</sub> yet still has sufficient sensitivity to this experiment indicates that the extent of boron aggregation on these materials must be higher (for the B-OH-containing sites) than the fresh B/SiO<sub>2</sub> materials. The breadth of the feature in the 1D "B DQ filtered NMR spectrum also spans to lower ppm values than the "B DQ filtered NMR spectrum reported for the fresh material shown in Figure 6c, suggesting that there are also "B nuclei without hydroxyl groups attached in the boron oxide aggregates on the spent material. We also note that the isotropic shift of the BO<sub>3</sub> feature for sites with B-OH groups shifts from ca. 16 ppm in the fresh materials to ca. 15 ppm in the spent materials (Figure 5, Table S1). Previous work on

borate glasses suggests that a shift to lower isotropic shifts indicates an increase in bridging oxide groups in borate materials.<sup>38</sup>

Through a combination of detailed IR, Raman, and NMR characterization, detailed structural information about the types of sites present on the surface of B/SiO<sub>2</sub> materials before and after catalytic testing was obtained. Table 1 summarizes the types of plausible surface sites on fresh and spent B/SiO<sub>2</sub> materials, along with the technique used to observe those species. In the fresh materials, we presume to have a mixture of isolated BO<sub>3</sub> sites with and without hydroxyl groups attached, chain-type metaborate type structures containing H-bonding B-OH groups, as well as some six-membered boroxol rings.

In the spent materials, we still plausibly have some isolated BO<sub>3</sub> sites with and without hydroxyl groups, and we also observe some chain-type metaborate-type structures, and a fraction of BO<sub>3</sub>OH sites. We expect that the average number of B atoms in the aggregated metaborate species is greater in the spent materials based on the shift of the features in the 1D  $^{11}$ B spectra to lower values for  $\delta_{100}$  (compared to the fresh material) and the increased sensitivity of the  $^{11}$ B DQ filtered NMR experiment in the spent material even at lower boron loadings. We do not see evidence for any appreciable amount of boroxol rings in the spent materials (based on Raman spectroscopy); therefore, we expect that these species degrade upon exposure to ODH conditions.

Table 1. Summary of plausible boron surface structures on fresh and spent B/SiO2 catalysts based on observations from IR, NMR, and Raman spectroscopic studies.

Catalysts	Identified Site	Experiment
Fresh B/SiO <sub>2</sub>	o <sup>, H</sup>	Transmission IR (v <sub>on</sub> at 3701 cm <sup>-1</sup> );
	(isolated BO <sub>2</sub> OH)	'H spin echo (2.7 ppm);  "B-'H D-RINEPT NMR (fraction of observed δ <sub>100</sub> ca. 15.9 ppm signal)
	(isolated BO <sub>3</sub> )	"B {'H dephased}NMR ( $\delta_{\omega}$ ca. 12.4 ppm)
	(chain-type metaborate)	Homonuclear 'H and 'B DQ-SQ NMR (broad 'H DQ-SQ peak at 4 ppm isotropic dimension; 'B DQ-SQ peak with δ <sub>so</sub> ca. 15.9 ppm)
	O-B O-B O O O O B O O O O O O O O O O O	Raman spectroscopy (ring breathing at 807 cm <sup>4</sup> at ≥ 200 °C dehydration)
Spent B/SiO <sub>2</sub>	(isolated BO <sub>2</sub> OH)	Transmission IR (v <sub>oi</sub> at 3701 cm <sup>-1</sup> ); <sup>1</sup> H spin echo (2.7 ppm); <sup>1</sup> B-iH D-RINEPT NMR (fraction of observed
	(isolated BO <sub>3</sub> )	$\delta_{\text{\tiny loo}}$ ca. 15.0 ppm signal)  "B {'H dephased}NMR (fraction of $\delta_{\text{\tiny loo}}$ ca. 12.2 ppm)
	QH and/or R A A A A A A A A A A A A A A A A A A	2D 'H-'H DQ-SQ NMR (broad peak at 4 ppm in isotropic dimension);  "B DQ-SQ NMR (wider peak breadth, Figure 7c)
	complex aggregate structures) $ \begin{array}{cccccccccccccccccccccccccccccccccc$	2D B-iH D-RINEPT (Correlation between B peak at 0 ppm and H peak at 8 ppm)
4 0 1 1	(BO <sub>i</sub> OH species)	

# 4. Conclusions

In this work we show that oxidized boron supported on an amorphous silica support is catalytically active for the oxidative dehydrogenation of propane, confirming the hypothesis that

the oxidized boron layer formed in situ on h-BN provides the active site. Like the h-BN and BNNTs, the B/SiO<sub>2</sub> materials contain agglomerated oxidized boron species. However, in h-BN and BNNTs, this oxidized phase is likely an extended overlayer generated by the oxidation and hydration of boron from the bulk of the material.18 For B/SiO<sub>2</sub>, these aggregates are simply made up of chains of BO<sub>3</sub> units that form from the decomposition of the B(OPr)<sub>3</sub> precursor during calcination and from rearrangement of the surface sites during ODH catalysis and thus cannot be replenished from the bulk support as might be the case for h-BN. Since both types of active materials contain aggregates, it is possible that multiple boron nuclei in close proximity (i.e., connected by bridging oxide groups) are required for these materials to be active for ODH. Additionally, we show that there is restructuring that occurs on the surface during the ODH reaction. The supposed dynamic nature of the active phase is in line with a recent computational study that predicts a highly dynamic active phase under reaction conditions. These insights suggest that a single-site catalysis model is not valid for this system and prompts further synthetic efforts to understand the requirements for active site formation. Therefore, a careful synthetic approach to generate single-site boron species (e.g., using grafting chemistry) would be instrumental to determine whether isolated boron species are viable catalysts. A catalyst such as this with more uniform structure would also help to more clearly define an 'active site' for ODH with these types of materials. This study acts as the foundational work for our understanding of supported boron oxides as ODH catalysts and will help inform strategies to synthesize catalysts with more monodisperse (i.e., having only one type) surface sites in the future. With this class of materials, we aim to work towards a more comprehensive structural understanding of the active boron species required for highly selective ODH catalysis.

# **Supporting Information**

The Supporting Information is available free of charge on the ACS Publications website at DOI: 10.1021/acs.jpcc.9b07429.

• Additional catalytic data, spectra, and NMR pulse programs (PDF)

Acknowledgments. Materials synthesis and characterization (A.M.L., M.C.C., P.U., C.K., and I.H.) were supported by the National Science Foundation under Grant No. CBET-1605101. Catalytic testing (W.P.M., S.P.B., T.A., and I.H.) was supported by U.S. Department of Energy under Grant No. DE-SC0017918. Solid-state NMR spectroscopy experiments (B.T. and A.J.R.) other than those shown in Figure 5 were supported by the National Science Foundation under Grant No. CBET-1916809. A.J.R. also thanks the Ames Laboratory Royalty Account and Iowa State University for additional funding. This study made use of the National Magnetic Resonance Facility at Madison, which is supported by NIH grants P41 GM103399 (NIGMS) and P41GM66326 (NIGMS). Additional equipment was purchased with funds from the University of Wisconsin, the NIH (RR02781, RR08438), the NSF (DMB-8415048, OIA-9977486, BIR-9214394), and the USDA.

#### References

- 1. Venegas, J. M.; McDermott, W. P.; Hermans, I. Serendipity in Catalysis Research: Boron-Based Materials for Alkane Oxidative Dehydrogenation. *Acc. Chem. Res* **2018**, *51*, 2556-2564.
- 2. Venegas, J. M.; Grant, J. T.; McDermott, W. P.; Burt, S. P.; Micka, J.; Carrero, C. A.; Hermans, I. Selective Oxidation of n-Butane and Isobutane Catalyzed by Boron Nitride. *ChemCatChem* **2017**, *9*, 2118-2127.
- 3. Shi, L.; Wang, D.; Song, W.; Shao, D.; Zhang, W.-P.; Lu, A.-H. Edge-hydroxylated Boron Nitride for Oxidative Dehydrogenation of Propane to Propylene. *ChemCatChem* **2017**, *9*, 1788-1793.
- 4. Lei Shi, B. Y., Dan Shao, Fan Jiang, Dongqi Wang, An-Hui Lu Selective Oxidative Dehydrogenation of Ethane to Ethylene over a Hydroxylated Boron Nitride Catalyst. *Chin. J. Catal.* **2017**, *38*, 389-395.
- 5. Huang, R.; Zhang, B.; Wang, J.; Wu, K.-H.; Shi, W.; Zhang, Y.; Liu, Y.; Zheng, A.; Schlögl, R.; Su, D. S. Direct Insight into Ethane Oxidative Dehydrogenation over Boron Nitrides. *ChemCatChem* **2017**, *9*, 3293-3297.
- 6. Guo, F.; Yang, P.; Pan, Z.; Cao, X.-N.; Xie, Z.; Wang, X. Carbon-Doped BN Nanosheets for the Oxidative Dehydrogenation of Ethylbenzene. *Angew. Chem., Int. Ed.* **2017,** *56*, 8231-8235.
- 7. Grant, J. T.; McDermott, W. P.; Venegas, J. M.; Burt, S. P.; Micka, J.; Phivilay, S. P.; Carrero, C. A.; Hermans, I. Boron and Boron-Containing Catalysts for the Oxidative Dehydrogenation of Propane. *ChemCatChem* **2017**, *9*, 3623-3626.
- 8. Grant, J. T.; Carrero, C. A.; Goeltl, F.; Venegas, J.; Mueller, P.; Burt, S. P.; Specht, S. E.; McDermott, W. P.; Chieregato, A.; Hermans, I. Selective Oxidative Dehydrogenation of Propane to Propene using Boron Nitride Catalysts. *Science* **2016**, *354*, 1570-1573.
- 9. Love, A. M.; Thomas, B.; Specht, S. E.; Hanrahan, M. P.; Venegas, J. M.; Burt, S. P.; Grant, J. T.; Cendejas, M. C.; McDermott, W. P.; Rossini, A. J. et al. Probing the Transformation of Boron Nitride Catalysts under Oxidative Dehydrogenation Conditions. *J. Am. Chem. Soc.* **2019**, *141*, 182-190.
- 10. Yasushi, M.; Kiyoshi, O.; Yuji, W.; Akira, M. Partial Oxidation of Ethane over Boron Oxide Added Catalysts. *Chem. Lett.* **1989**, *18*, 535-538.
- 11. Cucinieri Colorio, G.; Auroux, A.; Bonnetot, B. Acidity and Surface Behavior of Alumina-Boria Catalyst Studied by Adsorption Microcalorimetry of Probe Molecules. *Journal of Thermal Analysis and Calorimetry* **1993**, *40*, 1267-1276.
- 12. Colorio, G.; Védrine, J. C.; Auroux, A.; Bonnetot, B. Partial Oxidation of Ethane over Alumina-Boria Catalysts. *Appl. Catal.*, A **1996**, *137*, 55-68.
- 13. Buyevskaya, O. V.; Baerns, M. Catalytic Selective Oxidation of Propane. *Catal. Today* **1998,** *4*2, 315-323.
- 14. Buyevskaya, O. V., Muller, D., Pitsch, I., Baerns, M. In *Selective Oxidative Conversion of Propane of Olefins and Oxygenates on Boria-Containing Catalysts*, Fifth International Natural Gas Conversion Symposium, Taormina, Italy, Taormina, Italy, 1998.
- 15. Love, A. M.; Carrero, C. A.; Chieregato, A.; Grant, J. T.; Conrad, S.; Verel, R.; Hermans, I. Elucidation of Anchoring and Restructuring Steps during Synthesis of Silica-Supported Vanadium Oxide Catalysts. *Chem. Mater.* **2016**, *28*, 5495-5504.

- 16. Grant, J. T.; Love, A. M.; Carrero, C. A.; Huang, F.; Panger, J.; Verel, R.; Hermans, I. Improved Supported Metal Oxides for the Oxidative Dehydrogenation of Propane. *Top. Catal.* **2016**, *59*, 1545-1553.
- 17. Grant, J. T.; Carrero, C. A.; Love, A. M.; Verel, R.; Hermans, I. Enhanced Two-Dimensional Dispersion of Group V Metal Oxides on Silica. *ACS Catal.* **2015**, *5*, 5787-5793.
- 18. Zhang, Z.; Jimenez-Izal, E.; Hermans, I.; Alexandrova, A. N. Dynamic Phase Diagram of Catalytic Surface of Hexagonal Boron Nitride under Conditions of Oxidative Dehydrogenation of Propane. *J. Phys. Chem. Lett.* **2019**, *10*, 20-25.
- 19. Venegas, J. M.; Hermans, I. The Influence of Reactor Parameters on the Boron Nitride-Catalyzed Oxidative Dehydrogenation of Propane. *Organic Process Research & Development* **2018**, 22, 1644-1652.
- 20. Harris, R. K.; Becker, E. D.; Cabral de Menezes, S. M.; Goodfellow, R.; Granger, P. NMR Nomenclature: Nuclear Spin Properties and Conventions for Chemical Shifts: IUPAC Recommendations 2001. *Solid State Nuclear Magnetic Resonance* **2002**, *22*, 458-483.
- 21. Fung, B. M.; Khitrin, A. K.; Ermolaev, K. An Improved Broadband Decoupling Sequence for Liquid Crystals and Solids. *Journal of Magnetic Resonance* **2000**, *142*, 97-101.
- 22. Venkatesh, A.; Hanrahan, M. P.; Rossini, A. J. Proton Detection of MAS Solid-State NMR Spectra of Half-Integer Quadrupolar Nuclei. *Solid State Nuclear Magnetic Resonance* **2017**, 84, 171-181.
- 23. Trebosc, J.; Hu, B.; Amoureux, J. P.; Gan, Z. Through-Space R3-HETCOR Experiments between Spin-1/2 and Half-Integer Quadrupolar Nuclei in Solid-State NMR. *Journal of Magnetic Resonance* **2007**, *186*, 220-227.
- 24. Hu, B.; Trébosc, J.; Amoureux, J. P. Comparison of Several Hetero-nuclear Dipolar Recoupling NMR Methods to be used in MAS HMQC/HSQC. *Journal of Magnetic Resonance* **2008**, *192*, 112-122.
- 25. Yao, Z.; Kwak, H.-T.; Sakellariou, D.; Emsley, L.; Grandinetti, P. J. Sensitivity Enhancement of the Central Transition NMR Signal of Quadrupolar Nuclei under Magic-Angle Spinning. *Chem. Phys. Lett.* **2000**, *327*, 85-90.
- 26. Prasad, S.; Kwak, H.-T.; Clark, T.; Grandinetti, P. J. A Simple Technique for Determining Nuclear Quadrupole Coupling Constants with RAPT Solid-State NMR Spectroscopy. *J. Am. Chem. Soc.* **2002**, *124*, 4964-4965.
- 27. Wang, Q.; Trébosc, J.; Li, Y.; Xu, J.; Hu, B.; Feng, N.; Chen, Q.; Lafon, O.; Amoureux, J.-P.; Deng, F. Signal Enhancement of J-HMQC Experiments in Solid-State NMR Involving Half-Integer Quadrupolar Nuclei. *Chem. Commun.* **2013**, *49*, 6653-6655.
- 28. Zhao, X.; Sudmeier, J. L.; Bachovchin, W. W.; Levitt, M. H. Measurement of NH Bond Lengths by Fast Magic-Angle Spinning Solid-State NMR Spectroscopy: A New Method for the Quantification of Hydrogen Bonds. *J. Am. Chem. Soc.* **2001**, *123*, 11097-11098.
- 29. Zhuravlev, L. T. The Surface Chemistry of Amorphous Silica. Zhuravlev Model. *Colloids Surf.*, A **2000**, *173*, 1-38.
- 30. Gilson, T. R. Characterisation of Ortho- and Meta-Boric Acids in the Vapour Phase. *Journal of the Chemical Society, Dalton Transactions* **1991**, 2463-2466.
- 31. Andrews, L.; Burkholder, T. R. Infrared Spectra of Molecular B(OH)3 and HOBO in Solid Argon. *The Journal of Chemical Physics* **1992**, *97*, 7203-7210.
- 32. Krishnan, K. The Raman Spectrum of Boric Acid. *Proceedings of the Indian Academy of Sciences Section A* **1963**, *57*, 103-108.

- 33. Bezerra da Silva, M.; Santos, R. C. R.; Freire, P. T. C.; Caetano, E. W. S.; Freire, V. N. Vibrational Properties of Bulk Boric Acid 2A and 3T Polymorphs and Their Two-Dimensional Layers: Measurements and Density Functional Theory Calculations. *J. Phys. Chem. A* **2018**, *122*, 1312-1325.
- 34. Youngman, R. E.; Zwanziger, J. W. Network Modification in Potassium Borate Glasses: Structural Studies with NMR and Raman Spectroscopies. *J. Phys. Chem.* **1996**, *100*, 16720-16728.
- 35. Simon, G.; Hehlen, B.; Vacher, R.; Courtens, E. Hyper-Raman Scattering Analysis of the Vibrations in Vitreous Boron Oxide. *Physical Review B* **2007**, *76*, 054210.
- 36. Cory, D. G.; Ritchey, W. M. Suppression of Signals from the Probe in Bloch Decay Spectra. *Journal of Magnetic Resonance* (1969) **1988**, 80, 128-132.
- 37. Mackenzie, K., Smith, M., NMR of Other Commonly Studied Nuclei. In *Multinuclear Solid-State Nuclear Magnetic Resonance of Inorganic Materials*, Cahn, R., Ed. Elsevier: Amsterdam, 2002; Vol. 6, pp 420-432.
- 38. Kroeker, S.; Stebbins, J. F. Three-Coordinated Boron-11 Chemical Shifts in Borates. *Inorganic Chemistry* **2001**, *40*, 6239-6246.
- 39. Angel Wong, Y.-T. B., D.L, Recent Advances in 11B Solid-State Nuclear Magnetic Resonance Spectroscopy of Crystalline Solids. In *Annual Reports on NMR Spectroscopy*, Webb, G., Ed. 2018.
- 40. Müller, D.; Grimmer, A.-R.; Timper, U.; Heller, G.; Shakibaie-Moghadam, M. 11B-MAS-NMR-Untersuchungen zur Anionenstruktur von Boraten. Zeitschrift für anorganische und allgemeine Chemie 1993, 619, 1262-1268.
- 41. Schnell, I.; Spiess, H. W. High-Resolution 1H NMR Spectroscopy in the Solid State: Very Fast Sample Rotation and Multiple-Quantum Coherences. *Journal of Magnetic Resonance* **2001**, *151*, 153-227.
- 42. Feike, M.; Demco, D. E.; Graf, R.; Gottwald, J.; Hafner, S.; Spiess, H. W. Broadband Multiple-Quantum NMR Spectroscopy. *Journal of Magnetic Resonance, Series A* **1996,** *122*, 214-221.
- 43. Wiench, J. W.; Bronnimann, C. E.; Lin, V. S. Y.; Pruski, M. Chemical Shift Correlation NMR Spectroscopy with Indirect Detection in Fast Rotating Solids: Studies of Organically Functionalized Mesoporous Silicas. *J. Am. Chem. Soc.* **2007**, *129*, 12076-12077.
- 44. Mali, G.; Fink, G.; Taulelle, F. Double-Quantum Homonuclear Correlation Magic Angle Sample Spinning Nuclear Magnetic Resonance Spectroscopy of Dipolar-Coupled Quadrupolar Nuclei. *The Journal of Chemical Physics* **2004**, *120*, 2835-2845.
- 45. Edén, M. Homonuclear Dipolar Recoupling of Half-Integer Spin Quadrupolar Nuclei: Techniques and Applications. *Solid State Nuclear Magnetic Resonance* **2009**, *36*, 1-10.
- 46. Trébosc, J.; Wiench, J. W.; Huh, S.; Lin, V. S. Y.; Pruski, M. Solid-State NMR Study of MCM-41-type Mesoporous Silica Nanoparticles. *J. Am. Chem. Soc.* **2005**, *127*, 3057-3068.
- 47. Hansen, M. R.; Jakobsen, H. J.; Skibsted, J. Structure and Dynamics of Hydrous Surface Species on Alumina–Boria Catalysts and Their Precursors from 1H, 2H, 11B, and 27Al MAS NMR Spectroscopy. *J. Phys. Chem. C* **2009**, *113*, 2475-2486.
- 48. Hansen, M. R.; Jakobsen, H. J.; Skibsted, J. Structural Environments for Boron and Aluminum in Alumina–Boria Catalysts and Their Precursors from 11B and 27Al Single- and Double-Resonance MAS NMR Experiments. *J. Phys. Chem. C* **2008**, *112*, 7210-7222.

# TOC Graphic

